Atmos. Chem. Phys. Discuss., https://doi.org/10.5194/acp-2018-596
Manuscript under review for journal Atmos. Chem. Phys.
Discussion started: 19 July 2018

Atmospheric Chemistry and Physics Discussions

Kinetic mass-transfer calculation of water isotope fractionation due to cloud microphysics in a regional meteorological model

I-Chun Tsai[1], Wan-Yu Chen[2,3], Jen-Ping Chen*[2,4] and Mao-Chang Liang[5]

1. Research Center for Environmental Changes, Academia Sinica, Taipei, Taiwan R. O. C.
2. Department of Atmospheric Sciences, National Taiwan University, Taipei, Taiwan, R.O.C.
3. Central Weather Bureau, Taipei, Taiwan, R.O.C.
4. International Degree Program on Climate Change and Sustainable Development, National Taiwan University, Taipei, Taiwan, R.O.C.
5. Institute of Earth Sciences, Academia Sinica, Taipei, Taiwan R. O. C.

* Corresponding Author:
Jen-Ping Chen, Professor
Department of Atmospheric Sciences
National Taiwan University
No. 1, Sect. 4, Roosevelt Road, Taipei, Taiwan 10673
Email: jpchen@ntu.edu.tw
Phone: +886-2-33663912Fax: +886-2-23633317

Atmos. Chem. Phys. Discuss., https://doi.org/10.5194/acp-2018-596
Manuscript under review for journal Atmos. Chem. Phys.
Discussion started: 19 July 2018

Atmospheric Chemistry and Physics Discussions

Abstract

In conventional atmospheric models, isotope exchange between liquid and gas phases is usually assumed to be in equilibrium, and the highly kinetic phase transformation processes inferred in clouds are yet to be fully investigated. In this study, a two-moment microphysical scheme in the NCAR Weather Research and Forecasting (WRF) model was modified to allow kinetic calculation of isotope fractionation due to various cloud microphysical phase-change processes. A case of moving cold front is selected for quantifying the effect of different factors controlling isotopic composition, including water vapor sources, atmospheric transport, phase transition pathways of water in clouds, and kinetic versus equilibrium mass transfer. A base-run simulation was able to reproduce the ~50‰ decrease in δD that observed during the frontal passage. Sensitivity tests suggest that all the above factors contributed significantly to the variations in isotope composition. The thermal equilibrium assumption commonly used in earlier studies may cause an overestimate of mean vapor-phase δD by 11‰, and the maximum difference can be more than 20‰. Without microphysical fractionation, the δD in water vapor can be off by about 25‰. Also, using initial vertical distribution and lower boundary conditions of water isotopes from satellite data are critical to successful isotope simulations, without which the δD in water vapor can be off by about 34 and 28‰, respectively.

Atmos. Chem. Phys. Discuss., https://doi.org/10.5194/acp-2018-596
Manuscript under review for journal Atmos. Chem. Phys.
Discussion started: 19 July 2018

1 Introduction

The stable water isotopocules ($^{1}H_2O$, $^{1}H^{2}D^{16}O$ and $^{1}H_2{}^{18}O$) differ in molecular symmetry and weight. These differences in physical properties lead to a change in the stable isotope composition of water, due to fractionation during phase changes. When water vapor condenses and forms liquid or solid particles, it becomes depleted in ^{2}D and ^{18}O, because heavy isotopocules condense preferentially to light ones. Information about the stable isotopocules of water is thus useful for understanding the water cycle [*Dansgaard*, 1964; *Dawson and Ehleringer*, 1998; *Lorius et al.*, 1985; *Risi et al.*, 2012; *Sturm et al.*, 2010].

Isotope fractionation, as measured in precipitation, has been studied for decades. The observed isotope concentrations often exhibit significant variation in either time or location. Factors such as surface type (e.g., land versus ocean), latitude, temperature, and precipitation amount effects are commonly considered to be key to the relationship between isotope fractionation and meteorological parameters [*Dansgaard*, 1964; *Gonfiantini*, 1985; *Rozanski et al.*, 1993b; *Yurtsever and Gat*, 1981]. These factors are related to various physical processes, such as the surface water vapor source, atmospheric transport, phase changes in clouds and gravitational sorting of precipitation hydrometeors. For example, the water vapor source affects the concentration of different water isotopocules via evaporation and advection in the atmospheric boundary layer. On the other hand, vertical sorting of hydrometeors and cloud microphysical processes determine the exchange of isotopes between different phases. Untangling the intertwined effects of the various physical processes is essential to understanding isotope fractionation and the atmospheric water cycle.

The variations in isotope concentrations usually have multiple causes, and it is difficult to understand the impacts of different factors by measurements alone. Therefore, numerical models have been used to simulate isotope fractionation in the

atmosphere. The Rayleigh-type models, in which the air mass is continuously cooled down and the condensation process is assumed to occurr in isotopic equilibrium, are widely used in discussing isotope measurements [*Aldaz and Deutsch*, 1967; *Dansgaard*, 1964]. Such models can explain the linear relationship between the surface temperature and isotopic composition of precipitation [*Rozanski et al.*, 1993a], and have been expanded to incorporate more processes since the publication of *Dansgaard* [1964]. For example, *Jouzel and Merlivat* [1984] reported that the isotopic equilibrium assumption led to an overestimation of the temperature-isotope gradients of polar snow, so they included isotopic kinetic effects at snow formation in the models. However, the Rayleigh-type models greatly simplify the complexity of the hydrological cycle, and *Joussaume et al.* [1984] introduced the concept of building isotopes into an atmospheric general circulation model (AGCM).

AGCMs can calculate the transport and mixing of air masses from different sources (which cannot be addressed by the Rayleigh-type models), and have been used in studying the hydrological cycle in the troposphere [*Hoffmann et al.*, 1998; *Lee et al.*, 2007; *Sjolte and Hoffmann*, 2014; *Yoshimura et al.*, 2008]. In conventional AGCMs, isotope exchange between liquid and gas phases is usually assumed to be in a partial or full equilibrium state [*Hoffmann et al.*, 1998]. However, in a synoptic weather system such as a front or typhoon, thermal equilibrium fractionation may not be appropriate for describing fractionation during phase change because the clouds are usually not in vapor equilibrium [*Laskar et al.*, 2014].

To understand the role of different factors in the fractionation of the stable isotopes of water at the synoptic scale, this study developed a kinetic fractionation scheme water isotopocules using a two-moment microphysical scheme that coupled into the National Center for Atmospheric Research (NCAR) Weather Research and Forecasting (WRF) model [*Skamarock*, 2008]. Duterium is selected as an representative

isotopes, and the microphysical processes of deuterium such as condensation and collision were incorporated into WRF. A moving frontal system is selected to demonstrate the effect of microphysical fractionation versus other controlling factors such as air mass origins and surface sources. The effects of microphysical processes, including kinetic versus equilibrium treatments, are discussed in more details; whereas the importance of initial and boundary conditions of vapor-phase isotope is also investigated.

2 Methodology

In this study, the WRF model version 3.4.1 coupled with a two-moment bulkwater microphysical scheme [cf. *Cheng et al.*, 2010; *Chen et al.*, 2015; Dearden et al., 2016] that was developed at the National Taiwan University (hereafter, the NTU scheme) was selected for simulations. One of the advantages of the NTU scheme is that it does not assume "saturation adjustment" (i.e., all supersaturated vapor is forced to condense out) as in most microphysics schemes, so the condensation processes are calculated according to kinetic mass transfer principles. The HDO cycle and their initial and boundary conditions, were incorporated into the model. Isotope mass transfer between vapor-, liquid-, and ice-phase hydrometeors during microphysical processes such as evaporation, condensation, collection, freezing, and melting were considered explicitly (cf. Fig. 1). The fractionation processes and thermodynamic properties of HDO are described in section 2.1 and the simulation setup, and observation data are given in section 2.2 and 2.3, respectively.

2.1 Description of the isotopic microphysical model

Atmos. Chem. Phys. Discuss., https://doi.org/10.5194/acp-2018-596
Manuscript under review for journal Atmos. Chem. Phys.
Discussion started: 19 July 2018

Atmospheric Chemistry and Physics Discussions

97 Thermal equilibrium fractionation has been widely used in conventional models.
98 In such schemes, the HDO concentration can be determined from the H_2O
99 concentration for both gas and liquid phases, because it is assumed that HDO is always
100 in equilibrium with H_2O, irrespective of their phase states. The equilibrium between
101 stable isotopes in liquid water and vapor phases is commonly expressed using the
102 isotopic fractionation factor α_{l-v}:

103 $$\alpha_{l-v} \equiv \frac{R_l}{R_v} \quad (1)$$

104 where R is the ratio of the heavy (HDO) to light (H_2O) isotopes. This ratio can be
105 explained with the Raoult's law, which states that the activity (saturation ratio) of each
106 species in the vapor phase equals its activity in the liquid phase. For the HDO–H_2O
107 system, this relationship can be expressed as:

108 $$\frac{n_{HDO}}{n_{HDO}+n_{H2O}+n_x} = \frac{P_{HDO}}{P_{s,HDO}} \quad (2a)$$

109 $$\frac{n_{H2O}}{n_{HDO}+n_{H2O}+n_x} = \frac{P_{H2O}}{P_{s,H2O}} \quad (2b)$$

110 where n is the number of moles in the liquid phase, P is vapor pressure, P_s is
111 saturation vapor pressure, whereas x represents all other chemical species. By
112 dividing (2a) by (2b), one can derive the following:

113 $$\frac{\frac{n_{HDO}}{n_{H2O}}}{\frac{P_{HDO}}{P_{H2O}}} = \frac{P_{s,H2O}}{P_{s,HDO}} \quad (3)$$

114 One can see that the left-hand-side term is exactly α_{l-v}, while the right-hand-side
115 term tells us that this factor is actually the ratio between the saturation vapor pressure
116 of H_2O and HDO. Thus the isotopic fractionation factor α_{l-v} is a function of
117 temperature only, and can be determined experimentally. In this study, we adopted
118 the temperature dependence of α_{l-v} from *Horita and Wesolowski* [1994]:

119 $$10^3 \cdot ln\alpha_{l-v} = 1158\left(\frac{T^3}{10^9}\right) - 1620.1\left(\frac{T^2}{10^6}\right) + 794.84\left(\frac{T}{10^3}\right) - 161.04 + 2.9992\left(\frac{10^9}{T^3}\right) \quad (4a)$$

120

121 whereas that between ice and water vapor was adapted from *Ellehoj et al.* [2013].

122 $$ln\alpha_{s-v} = ln\frac{R_s}{R_v} = 0.2133 - \frac{203.10}{T} + \frac{48888}{T^2} \quad (4b)$$

123 where the subscript "s" means solid phase.

124 When kinetic process is considered, isotopic fractionation is not only related to
125 temperature but also factors such as the diffusion coefficient and water vapor
126 concentration. The calculation of kinetic fractionation during
127 condensation/evaporation is based on the two-stream Maxwellian kinetic equation:

128 $$\frac{dm_{HDO}}{dt} = 4\pi r D_{HDO}\left(\rho_{env,HDO} - \rho_{p,HDO}\right) \quad (5)$$

129 where m is HDO mass in the particle, t is time, r is hydrometeor particle size, D
130 is the mass diffusivity in air, ρ_{env} is vapor density in the air, and ρ_p is vapor density
131 at the particle surface. The latter two terms can be rewritten as:

132 $$\rho_{env,HDO}=\frac{P_{HDO}}{R_{HDO}T_{air}} \text{ and } \rho_{p,HDO} = a_{HDO}\frac{P_{s,HDO}}{R_{HDO}T_p} \quad (6)$$

133 where R_{HDO} is the gas constant of HDO; a_{HDO} and $P_{s,HDO}$ are the liquid-phase
134 activity and saturation vapor pressure of HDO, respectively; and T_{air} and T_p are
135 temperatures of air and particle surface, respectively.

136 Equation (5) is for single droplet, but the bulkwater microphysical schemes
137 commonly used in regional weather model deal with a population of droplets (thus
138 called bulkwater). The NTU microphysical scheme that applied in this study provided
139 a parameterization for the condensation growth of a population of cloud drops and
140 raindrops, which are modified to handle HDO by replacing key parameters such as the
141 HDO saturation vapor pressure, $P_{s,HDO}$, and diffusion coefficient, D_{HDO}. The HDO
142 saturation pressure, which is needed for the kinetic mass transfer calculation in Eq. (5),
143 can be obtained by equating Eq. (3) to Eq. (4). The derived HDO saturation vapor

144 pressure is generally lower than that of H_2O, and the differences increase as
145 temperature gets lower (Fig. 2). Noted that because the α_{l-v} of ^{18}O (grey line in Fig.
146 2) does not deviate significantly from unity, we focus on deuterium for demonstrating
147 the fractionation processes.

148 The mass diffusivity of HDO in air, D_{HDO}, in Eq. (5) was obtained based on the
149 relationship proposed by *Hirschfelder et al.* [1954]:

150 $$D_x \propto \frac{m_{Air}+m_x}{m_{Air}m_x} \quad (7)$$

151 where x represents any gas molecule. Assuning that the proportionality constants
152 are the same for D_{HDO} and D_{H_2O}, one can obtained the following:

153 $$\frac{D_{HDO}}{D_{H_2O}} = \frac{\frac{m_{Air}+m_{HDO}}{m_{Air}m_{HDO}}}{\frac{m_{Air}+m_{H_2O}}{m_{Air}m_{H_2O}}} \cong 0.9676 \quad (8)$$

154 with which we can relate D_{HDO} to D_{H_2O}.

155 For vapor deposition, sublimation, and other processes connected with vapor–
156 solid phase change, the α_{s-v} in Eq. (4b) was used to calculate the saturation vapor
157 pressure of HDO with respect to HDO ice. For processes of collision-collection or
158 melting/freezing, the masses of isotopes of the involving particles are simply
159 combined or conserved, respectively, without worrying about thermodynamic
160 equilibrium.

161

162 2.2 Simulation Setup

163 Frontal systems are not only rich in cloud microphysical processes but also involve
164 air-mass transitions and atmospheric circulation. As a result, they are ideal for
165 evaluating the relative contribution of various physical processes to isotopic
166 fractionation. The case selected for this study is a frontal system that passed through

northern Taiwan on 11 June 2012, with moderate to heavy rainfall from the night of 11 June until noon on 12 June. Special focus will be placed on northern Taiwan because of the availability of isotope measurements for verification.

The simulation domain is shown in Fig. 3. The resolution of the coarse domain was set at 81 km, covering the region from 90° to 150°E and 0° to 50°N. The resolutions of the nested domains were set at 27 km, 9 km, and 3 km. The innermost domain covers Taiwan and the surrounding ocean. Twenty-eight vertical layers were used, eight of which were below 1.5 km (roughly the height of the planetary boundary layer), with a maximum model height at 50 hPa. For the initial and boundary conditions, we applied the National Centers for Environmental Prediction (NCEP) Final Global analysis (FNL) data with a 1° by 1° resolution. FNL data for wind properties and temperatures were nudged into domains 1 and 2 every 6 h for better simulation of the meteorology. The physical options used in the WRF model included the NTU microphysical scheme, the rapid radiative transfer model (RRTM) longwave and short wave radiation scheme [*Mlawer et al.*, 1997], and the Yonsei University (YSU) planetary boundary layer scheme [*Hong et al.*, 2006]. Cumulus parameterization was turned off in the simulations.

To examine different factors that control the isotopocules concentration, six simulations were conducted: the control run (CTRL) used the kinetic approach for cloud microphysical processes; the EQ run used the thermal equilibrium approach; NoIce was conducted to examine the differences between liquid- and ice-phase fractionations; NoLnd inspects land-sea contrast of water vapor sources; and NoVh is for investigating the vertical exchange of isotope composition between lower and upper troposphere. We also conducted a blank test (NoFrac) in which isotopic microphysical fractionation was turned off. Descriptions of these numerical experiments is listed in Table 1.

Atmos. Chem. Phys. Discuss., https://doi.org/10.5194/acp-2018-596
Manuscript under review for journal Atmos. Chem. Phys.
Discussion started: 19 July 2018

Atmospheric Chemistry and Physics Discussions

193 The isotopic value for water vapor or condensates is conventionally expressed as
194 δD in ‰:

195 $$\delta D = \left(\frac{R}{R_{SMOW}} - 1\right) \cdot 1000 \quad (9)$$

196 where *R* is the $\frac{HDO}{H_2O}$ ratio in the sample, and R_{SMOW} is the Vienna Standard Mean Ocean
197 Water isotopic ratio [*Craig*, 1961]. The lower boundary condition of δD is
198 calculated by relating HDO flux to H_2O flux according to Eqs. (3) and (4). In such as
199 conversion, the ratio R_l is set to be that in surface precipitation according to
200 observational values provided by the Global Network of Isotopes in Precipitation (GNIP)
201 [*Johnson and Ingram*, 2004; *Rozanski et al.*, 1993b]. The obtained initial near-surface
202 distribution of water vapor δD (δD_V) is shown in Fig. 4a.

203 The vertical distribution of initial atmospheric water isotope concentrations (Fig.
204 4b) was obtained from the NASA TES-Aura level-3 data
205 (http://tes.jpl.nasa.gov/data/products/). We took the data for the month of June
206 and averaged over years 2006-2009. Although water vapor concentration (QV)
207 usually decrease exponentially with height, the ratio between the HDO concentration
208 (QIV) and QV changes rather linearly with height. So, for areas over land, the vertical
209 profile is fitted as the following:

210 $$\mathrm{QIV(z)} = \left(\frac{QIV_{srf}}{QV_{srf}}\right) \cdot (-4.940699 \cdot 10^{-5} \cdot \mathrm{z} + 1.128299) \cdot \mathrm{QV(z)} \quad (10a)$$

211 where QIV_{srf} and QV_{srf} are near surface value of QIV and QV, respectively. For
212 marine environments, the profile is fitted as:

213 $$\mathrm{QIV(z)} = \left(\frac{QIV_{srf}}{QV_{srf}}\right) \cdot (-5.005261 \cdot 10^{-5} \cdot \mathrm{z} + 1.134024) \cdot \mathrm{QV(z)} \quad (10b)$$

214 Note that these formulas apply only to the free troposphere; within the planetary

boundary layers, QIV is assumed to be well mixed (see Fig. 4b for the full profiles).

2.3 Observations

The isotopic water vapor and rainwater δD data from 11–12 June, 2012, were recorded using a cavity ring-down spectroscopy analyzer (CARDS, Picarro L2120-i), following *Gupta et al.* [2009]. The measurement of rainwater was conducted on the fourth floor of the building of the Department of Geography, National Taiwan University (NTU, 25.02°N, 121.53°E). The isotopic water vapor measurements were conducted at Academia Sinica (AS), which is about 10 km east of the rainwater collection site. The two sites are marked as N and A, respectively, in Fig. 5a. The uncertainties in δD for liquid and vapor samples were found to be less than 0.3‰ and 1.0‰, respectively [*Laskar et al.*, 2014]. The precision of water vapor concentration measurements made using a Picarro CRDS is less than 100 ppmv [*Crosson*, 2008]; this is applicable to all of the data presented here. In addition to these experimental data, the NCEP Reanalysis II (R2) data and precipitation data from the Central Weather Bureau of Taiwan were used to verify the simulations.

3 Results

3.1 Model verification

Comparison of the model results with the NCEP R2 data shows that the model captured the locations of the cold front and associated low-pressure system reasonably well; the front was over the East China Sea on 11 June and moved to Taiwan on 12 June (Fig. 6). However, the simulated precipitation was generally lower than observed, especially over northwestern Taiwan (Fig. 5a). Additionally, the first peak in rainfall during the early morning of 11 June (Fig. 5b), was not obvious in the simulated results. The impact of these discrepancies will be discussed in section 4.

Atmos. Chem. Phys. Discuss., https://doi.org/10.5194/acp-2018-596
Manuscript under review for journal Atmos. Chem. Phys.
Discussion started: 19 July 2018

241 The observed δD_V was about −90~−120‰ during the pre- and post-frontal
242 periods, and decreased to a minimum of −160‰ on 12 June. The simulated δD_V
243 (−70~−100‰) were about 20‰ higher than observed during the pre- and post-frontal
244 periods (Fig. 7), whereas the minimum δD_V of −150‰ was slightly higher than the
245 observed during the rainy period. Observation of δD in precipitation (δD_L) was
246 available only after 09:00 (local time) on 12 June (Fig. 7b). It decreased slightly from -
247 70 to −90‰ before 16:00 and then recovered to around −30‰ by the evening of 12
248 June. The simulated minimum is also around −90‰, but occurred a few hours earlier
249 than observed. Overall, the model captured reasonably well the pattern and
250 magnitude of changes in δD during the frontal passage, except that the timing is off by
251 a few hours.
252
253 3.2 Factors affecting isotopic fractionation
254 The simulated spatial distribution of δD_V in Fig. 8a and 8d show two main zones
255 of minimum δD_V, one over mid-latitudes and the other over the latitudes of Taiwan.
256 The former is mainly due to low δD of surface vapor source (cf. Fig. 4a); whereas the
257 latter is associated with the frontal rainband, and correcponds to the observed minima
258 shown in Fig. 7a. At a first glance, one may deduce two main causes for the minima.
259 Firstly, the near surface air in the frontal zone is basically of continental origin, where
260 the δD_V is lower than over the oceans (cf. Fig. 4a). Secondly, strong microphysical
261 fractionation inside the frontal clouds caused a strong reduction (fractionation) in δD
262 of hydrometeors as can be seen in Figs. 8e and 8f; therefore, the evaporation of
263 hydrometeors would produce low δD_V in the lower troposphere. Note that the
264 location of the hydrometeor's δD minima at 500hPa and 850hPa is shifted due to the
265 structure of the frontal system. However, the relatively high δD_V behind (to the north
266 of) the frontal system may seem a bit strange, as the air mass there should be of

Atmos. Chem. Phys. Discuss., https://doi.org/10.5194/acp-2018-596
Manuscript under review for journal Atmos. Chem. Phys.
Discussion started: 19 July 2018

Atmospheric Chemistry and Physics Discussions

continental origin. This suggests more complicated mechanimss. Besides the water vapor source and microphysical fractionation, other factors such as the initial vertical distribution may also contribute to the variation in δD values. So, in order to decipher all possible controlling factors and to evaluate their relative contributions, we need to examine results from the 5 sensitivity experiments that listed in Table 1.

The most obvious differences between the CTRL and other simulations in terms of δD in the vapor (δD_V) and liquid (δD_L) phases at 850 hPa occurred near the front, because that is the location of the richest microphysical fractionation and largest contrast in air mass properties (Fig. 9). Isotopic fractionation due to phase change in the CTRL run was weaker than that calculated in the EQ run (Fig. 9a), because the isotopic compositions were not always in equilibrium between the different phases in the CTRL run. That led to slower isotopic fractionation under severe phase changes.

The vertical distribution of δD_V between the CTRL and EQ runs over northern Taiwan is shown in Fig. 10a. The differences in water vapor δD at around 850 hPa or higher prior to the passing of the front (point A, Fig. 10a) are associated with cloud formation due to mesoscale lifting in the warm air sector. When the frontal system passed through northern Taiwan in the early morning of 12 June, significant δD_L extended almost down to the surface. The δD_L in the EQ run was about 30‰ lower than that in the CTRL run during this period. These results suggest that the equilibrium assumption may lead to large discrepancy in δD for a synoptic-scale weather system, and kinetic calculation is crucial to isotope modeling.

The degree of isotopic fractionation is related to temperature. As the ratio between the saturation pressure of H_2O and HDO in different phases deviate more from unity at lower temperatures (cf. Fig. 2), higher degree of fractionation will occur at lower temperatures. The significance of ice-phase fractionation is tested with the NoIce run, for which the saturation vapor pressure of ice-phase HDO was assumed to

be the same as that of the liquid phase, which leads to weaker HDO vapor deposition on ice. The resulting differences in δD_V are small near the surface (Figs 9b and 10b), but become significant at higher altitudes where.the ice fractionation deviate more from that of liquid. Reduced δD in the ice phase (δD_I) can be seen immediately above the 0°C level (Fig. 10b), causing more heavier isotopocules to remain in the gas phase and then transport to higher altitudes. This results in an elevated δD in both the vapor and the ice phase. The increase in δD_V and δD_I can reach over 50‰ and 30‰, respectively, near the tropopause. Such changes may also affect the lower troposphere, because snow and graupel particles may fall to lower levels and bring down high δD_I water. The amount of changes due to such gravitational sorting depends on whether snow/graupel were formed in the lower or higher mixed-phase zone; the former leads to lower δD_V, while the latter increases it. However, the changes were generally within 10‰. Due to the temperature dependence of the isotopic value and the structure of the atmosphere, ignoring the difference between liquid and ice-phase fractionations will lead a vertical redistribution of the isotopes.

The initial and boundary conditions are also important in determining the isotope levels. Based on the IAEA data, precipitation δD decreases from marine to inland areas, indicating that the water source is important in determining the initial water isotope content. In the NoLnd run, the initial δD over land was set to be the same as that over the ocean, and this resulted in a higher δD not only over land but also in the frontal system (Fig. 9c). Ahead of the front, the vapor-phase δD in the NoLnd run increased by about 40‰ relative to the CTRL run. The initial vertical distribution of δD_V, which was based on satellite data, showed large vertical decay into the free troposphere. In the NoVh run, the initial δD in the free troposphere is assumed to be the same as that in the planetary boundary layer. This caused 20-50‰ overestimation of δD_V at near surface(Fig. 9d).

When the observed and simulated δD_V at AS and precipitation δD_L at NTU are compared (Fig. 11), one can see that the full simulation (i.e., the CTRL run, red line) is rather close to the observation in terms of the peak values during the time of frontal passage (06:00-12:00 LST on June 12). In contrast, δD_V was overestimated by 11‰ in the equilibrium run, and underestimated by 28 and 34‰ in the NoLnd and NoVh runs, respectively. The simulated δD_V in the NoIce run is rather close to that in the CTRL run, which is consistent with the vertical profile shown in Fig. 10b, suggesting that the ice-phase process does not have a significant effect on δD at lower altitudes; however, the changes in the upper troposphere are significant.

4 Discussion

Information about the stable isotopocules of water can be used to understand the water cycle. For example, the observed δD_V decreased after 06:00 on 12 June (black line in Fig. 11), much later than the onset of the precipitation. This suggests that the source of water vapor before this time is the ocean, and that the microphysical processes related to the precipitation did not substantially affect δD_V during this period.

Model simulations can help with further understanding of such isotopic fractionation. The δD_V on 11 June varied little among different tests (Fig, 11) becasue the airmass was from nearby areas (i.e., no significant advection effect) and no cloud microphysical processes occurred during this period. However, water vapor δD_V decreased from -80 to -100‰ at mid night of 11-12 June in the control run, but not in the NoLnd run, indicating that the decreases in δD_V was due to advedction of the continental airmass. When the front passed through during the early morning of 12 June, δD_V decreased from −100 to −170‰ in the control run but not in the NoFrac run (grey line in Fig.10a), indicating that the additional differences was caused by cloud

345 microphysical processes. After the passage of frontal system, δD_V returned to its
346 background level, around −80‰. The results of these sensitivity tests suggest that the
347 changes in δD_V due to cloud microphysical processes, initial vertical distribution, and
348 lower boundary conditions are of a similar order, and are all important to isotopic
349 fractionation.

350 Although the model seem to adequately reproduced changes in δD in this frontal
351 case, there are some minor inconsistencies between the simulation results and
352 observations. Some discrepancies originated from the meteorological model itself and
353 the meteorological initial conditions, which caused inaccuracies in the intensity or
354 timing of surface precipitation. In fact, most models including ours failed to simulate
355 the strong precipitation over land for this system (Wang et al. 2016). The observed
356 water vapor and precipitation δD values were not in phase, and the water vapor δD
357 decreased prior to precipitation (black line in Fig. 11). In contrast, the decreases in the
358 simulated precipitation and water vapor δD were almost simultaneous, starting
359 around 03:00 on 12 June (red line in Fig. 11). This again suggests that the model missed
360 an earlier local convection system occurred during the early morning, such that the
361 simulation can reflect only the δD variation due to the frontal system. The simulated
362 δD_V decreased and returned to its previous level earlier than the observed δD_V
363 (~03:00-10:00 compared to ~07:00 -13:00). This also suggests that the arrival time of
364 the frontal system to Taipei was earlier than observed, although the speed of the
365 simulated system was close to that of the observed one, taking about seven hours to
366 pass through Taipei.

367 Uncertainties may also exist in the observation data, as the vapor and
368 precipitation measurements were taken at different locations, separated by about 10
369 km. A comparison of precipitation at different sites (Fig. 12; NanGang station is close
370 to AS and GongGuan station is close to NTU) suggests that the difference in sampling

371 locations would not significantly affect the results in this study. Another uncertainity is
372 that the isotopic value for water vapor at the lower boundary condition was assumed
373 to be in equilibrium with surface precipitation. *Rangarajan et al.* [2017] analyzed the
374 isotopic ratios in water vapor from measurements over Taipei, and they found that
375 isotopic values were not always in equilibrium. This suggests that the assumed lower
376 boundary condition might not always be applicable for Taipei. Moreover, since the
377 lower boundary condition can be affected by fresh precipitation, the modeled δD_V
378 might decrease after the precipitation event which brings in low δD_L to the soil; yet,
379 our model does not update the surface δD_V flux accordingly. This might partially
380 explain the discrepancy in δD_V after the frontal passage that shown in Fig. 7a.
381
382 5 Conclusion
383 Exploring physical processes controlling the stable isotopic composition of water,
384 including details such as water vapor source, atmospheric circulation, and cloud
385 microphysical processes, is useful for understanding the water cycle. In this study, we
386 modified the NCAR WRF model to understand the role of different factors in the
387 fractionation of the stable isotopes of water. The experimental stable isotope thermal
388 equilibrium data were converted into isotope saturation vapor pressure, which was
389 then used in the two-stream Maxwellian kinetic equation for calculating the
390 condensation/evaporation or deposition/sublimation of HDO, in parallel with that for
391 H_2O. Mass conservation was also considered explicitly for the collection processes as
392 well as during freezing/melting.
393 A frontal system event was selected to reveal the complexity of isotope
394 fractionation. The model captured the location of the front adequately, although the
395 estimated precipitation was less than observed. The simulated results showed fairly
396 good agreement with water vapor and rainwater isotope measurements, and

suggested that the decreases in water vapor δD before the front arrived in Taiwan was due to an airmass of continental origin. When the front passed during the early morning of 12 June, both the water vapor sources and the cloud microphysical processes contributed to a decrease in water vapor δD, which returned to a background levels after the front had passed.

Additional sensitivity experiments showed that the thermal equilibrium assumption commonly used in earlier studies might significantly overestimate mean δD by about 11‰, while the maximum difference can be more than 20‰, during the precipitatin event. Cloud microphysical processes, including ice-phase processes, have substantial effects on isotopic fractionation, especially on the vertical redistribution of isotopes. Furthermore, the sensitivity tests suggest that the initial vertical profile and the land–sea contrast in surface sources are quite important in simulating atmospheric stable isotopic composition, and should be estimated from observations such as satellite data, without which the underestimation in water vapor δD could reach about 34 and 28‰, respectively. In summary, this study suggest that a better understanding in the relationship between water isotope variation and hydrological cycle can be achieved with a combination of multi-platform observations and detailed cloud model simulations.

416 **References**

417 Aldaz, L., and S. Deutsch (1967), On a relationship between air temperature and
418 oxygen isotope ratio of snow and firn in the south pole region, *Earth and*
419 *Planetary Science Letters*, *3*(Supplement C), 267-274,
420 doi:https://doi.org/10.1016/0012-821X(67)90047-7.
421 Chen, J. P., and S. T. Liu (2004), Physically based two-moment bulkwater
422 parametrization for warm-cloud microphysics, *Quarterly Journal of the Royal*
423 *Meteorological Society*, *130*(596), 51-78, doi:10.1256/qj.03.41.
424 Chen, S. H., Y. C. Liu, T. R. Nathan, C. Davis, R. Torn, N. Sowa, C. T. Cheng, and J. P. Chen
425 (2015), Modeling the effects of dust-radiative forcing on the movement of
426 Hurricane Helene (2006), *Quarterly Journal of the Royal Meteorological Society*.
427 Cheng, C.-T., W.-C. WANG, and J.-P. CHEN (2007), A modelling study of aerosol impacts
428 on cloud microphysics and radiative properties, *Quarterly Journal of the Royal*
429 *Meteorological Society*, *133*(623B), 15.
430 Cheng, C.-T., W.-C. Wang, and J.-P. Chen (2010), Simulation of the effects of increasing
431 cloud condensation nuclei on mixed-phase clouds and precipitation of a front
432 system, *Atmospheric Research*, *96*(2–3), 461-476,
433 doi:10.1016/j.atmosres.2010.02.005.
434 Craig, H. (1961), Isotopic Variations in Meteoric Waters, *Science*, *133*(3465), 1702-1703,
435 doi:10.1126/science.133.3465.1702.
436 Crosson, E. R. (2008), A cavity ring-down analyzer for measuring atmospheric levels of
437 methane, carbon dioxide, and water vapor, *Applied Physics B*, *92*(3), 403-408,
438 doi:10.1007/s00340-008-3135-y.
439 Dansgaard, W. (1964), Stable isotopes in precipitation, *Tellus*, *16*(4), 436-468,
440 doi:10.1111/j.2153-3490.1964.tb00181.x.
441 Dawson, T. E., and J. R. Ehleringer (1998), Plants, isotopes and water use: a catchment-
442 scale perspective, *Isotope tracers in catchment hydrology*, 165-202.
443 Dearden, C, G. Vaughan, T.-C. Tsai, and J.-P. Chen, 2016: Exploring the diabatic role of ice
444 microphysical processes in UK summer cyclones. *Mon. Wea. Rev.*, **144**, 1249-1272.
445 Ellehoj, M., H. C. Steen-Larsen, S. J. Johnsen, and M. B. Madsen (2013), Ice-vapor
446 equilibrium fractionation factor of hydrogen and oxygen isotopes: Experimental
447 investigations and implications for stable water isotope studies, *Rapid*
448 *Communications in Mass Spectrometry*, *27*(19), 2149-2158.
449 Gonfiantini, R. (1985), On the isotopic composition of precipitation in tropical stations
450 (*), *Acta Amazonica*, *15*(1-2), 121-140.
451 Gupta, P., D. Noone, J. Galewsky, C. Sweeney, and B. H. Vaughn (2009), Demonstration
452 of high-precision continuous measurements of water vapor isotopologues in
453 laboratory and remote field deployments using wavelength-scanned cavity ring-

down spectroscopy (WS-CRDS) technology, *Rapid communications in mass spectrometry*, *23*(16), 2534-2542.

Hirschfelder, J. O., C. F. Curtiss, R. B. Bird, and M. G. Mayer (1954), *Molecular theory of gases and liquids*, Wiley New York.

Hoffmann, G., M. Werner, and M. Heimann (1998), Water isotope module of the ECHAM atmospheric general circulation model: A study on timescales from days to several years, *Journal of Geophysical Research: Atmospheres*, *103*(D14), 16871-16896, doi:10.1029/98JD00423.

Hong, S.-Y., Y. Noh, and J. Dudhia (2006), A New Vertical Diffusion Package with an Explicit Treatment of Entrainment Processes, *Monthly Weather Review*, *134*(9), 2318-2341, doi:10.1175/MWR3199.1.

Horita, J., and D. J. Wesolowski (1994), Liquid-vapor fractionation of oxygen and hydrogen isotopes of water from the freezing to the critical temperature, *Geochimica et Cosmochimica Acta*, *58*(16), 3425-3437.

Johnson, K. R., and B. L. Ingram (2004), Spatial and temporal variability in the stable isotope systematics of modern precipitation in China: implications for paleoclimate reconstructions, *Earth and Planetary Science Letters*, *220*(3), 365-377.

Joussaume, S., R. Sadourny, and J. Jouzel (1984), A general circulation model of water isotope cycles in the atmosphere, *Nature*, *311*, 24, doi:10.1038/311024a0.

Jouzel, J., and L. Merlivat (1984), Deuterium and oxygen 18 in precipitation: Modeling of the isotopic effects during snow formation, *Journal of Geophysical Research: Atmospheres*, *89*(D7), 11749-11757, doi:10.1029/JD089iD07p11749.

Laskar, A. H., J.-C. Huang, S.-C. Hsu, S. K. Bhattacharya, C.-H. Wang, and M.-C. Liang (2014), Stable isotopic composition of near surface atmospheric water vapor and rain–vapor interaction in Taipei, Taiwan, *Journal of hydrology*, *519*, 2091-2100.

Lee, J.-E., I. Fung, D. J. DePaolo, and C. C. Henning (2007), Analysis of the global distribution of water isotopes using the NCAR atmospheric general circulation model, *Journal of Geophysical Research: Atmospheres*, *112*(D16), n/a-n/a, doi:10.1029/2006JD007657.

Lorius, C., C. Ritz, J. Jouzel, L. Merlivat, and N. Barkov (1985), A 150,000-year climatic record from Antarctic ice, *Nature*, *316*, 591-596.

Mlawer, E. J., S. J. Taubman, P. D. Brown, M. J. Iacono, and S. A. Clough (1997), Radiative transfer for inhomogeneous atmospheres: RRTM, a validated correlated-k model for the longwave, *Journal of Geophysical Research: Atmospheres*, *102*(D14), 16663-16682, doi:10.1029/97JD00237.

Rangarajan, R., A. H. Laskar, S. K. Bhattacharya, C.-C. Shen, and M.-C. Liang (2017), An insight into the western Pacific wintertime moisture sources using dual water

vapor isotopes, *Journal of Hydrology*, *547*, 111-123.

Risi, C., et al. (2012), Process-evaluation of tropospheric humidity simulated by general circulation models using water vapor isotopologues: 1. Comparison between models and observations, *Journal of Geophysical Research: Atmospheres*, *117*(D5), D05303, doi:10.1029/2011JD016621.

Rozanski, K., L. Araguás-Araguás, and R. Gonfiantini (1993a), Isotopic Patterns in Modern Global Precipitation, in *Climate Change in Continental Isotopic Records*, edited, pp. 1-36, American Geophysical Union, doi:10.1029/GM078p0001.

Rozanski, K., L. Araguás-Araguás, and R. Gonfiantini (1993b), Isotopic patterns in modern global precipitation, *Climate change in continental isotopic records*, 1-36.

Sjolte, J., and G. Hoffmann (2014), Modelling stable water isotopes in monsoon precipitation during the previous interglacial, *Quaternary Science Reviews*, *85*, 119-135.

Skamarock, W. C., J. B. Klemp, J. Dudhia, D. O. Gill, D. M. Barker, M. Duda, X.-Y. Huang, W. Wang and J. G. Powers (2008), A Description of the Advanced Research WRF Version 3, *NCAR Technical Note*.

Sturm, C., Q. Zhang, and D. Noone (2010), An introduction to stable water isotopes in climate models: benefits of forward proxy modelling for paleoclimatology, *Climate of the Past*, *6*(1), 115-129.

Yoshimura, K., M. Kanamitsu, D. Noone, and T. Oki (2008), Historical isotope simulation using Reanalysis atmospheric data, *Journal of Geophysical Research: Atmospheres*, *113*(D19), n/a-n/a, doi:10.1029/2008JD010074.

Yurtsever, Y., and J. R. Gat (1981), Atmospheric waters, *of: IAEA (ed), Stable Isotope Hydrology: Deuterium and Oxygen-18 in the Water Cycle. Vienna: IAEA*, 103-142.

Atmos. Chem. Phys. Discuss., https://doi.org/10.5194/acp-2018-596
Manuscript under review for journal Atmos. Chem. Phys.
Discussion started: 19 July 2018

Atmospheric Chemistry and Physics Discussions

518 Table 1. Description of the 6 numerical experiments conducted in this study.

519

Abbreviation	Description
CTRL	All processes are included.
EQ	The isotopic fractionation between difference phases is in thermodynamic equilibrium.
NoIce	The isotopic fractionation between solid and other phases is the same as that of liquid and other phases (i.e., assuming the vapor pressure of solid HDO is the same as that of liquid HDO).
NoLnd	The initial δD over land is set to be the same as those over the ocean.
NoVh	The initial δD in the free troposphere was equal to that in the planetary boundary layer (i.e., no vertical gradient).
NoFrac	No isotopic fractionation considered in cloud microphysical processes (i.e., HDO is treated as a tracer).

520

521

Atmos. Chem. Phys. Discuss., https://doi.org/10.5194/acp-2018-596
Manuscript under review for journal Atmos. Chem. Phys.
Discussion started: 19 July 2018

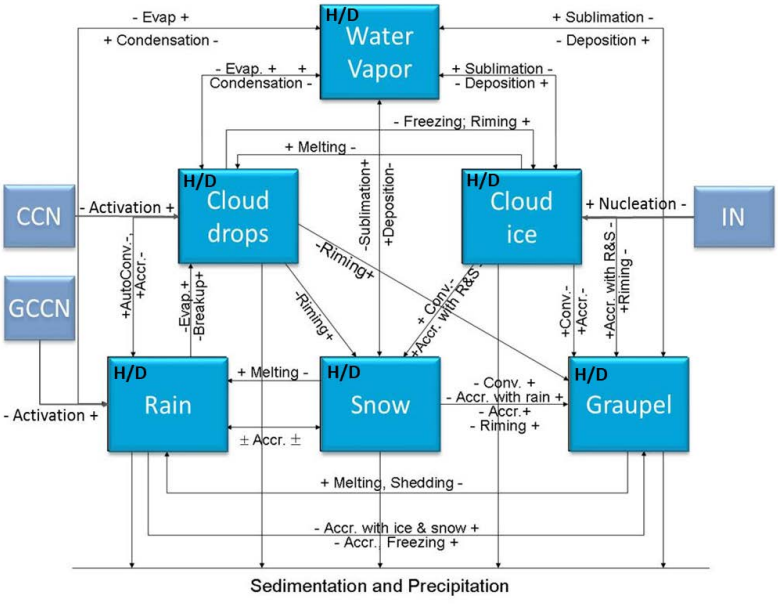

Figure 1. Schematics of modified NTU scheme. The blue boxes are the hydrometeors considered in the model and the H/D indicated that both H_2O and HDO are included. The arrows are the microphysical processes considered and the light blue boxes are condensation nuclei and ice nuclei. (Figure modified from Cheng et al. 2010)

Atmos. Chem. Phys. Discuss., https://doi.org/10.5194/acp-2018-596
Manuscript under review for journal Atmos. Chem. Phys.
Discussion started: 19 July 2018

Atmospheric Chemistry and Physics Discussions

528

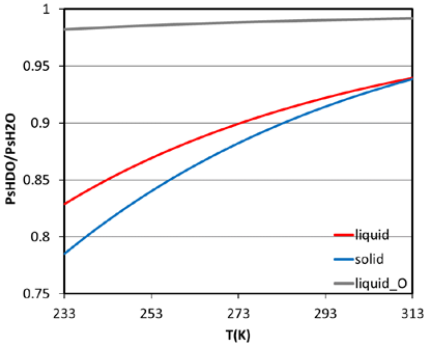

529

530 Figure 2. The ratio between saturation pressure of H_2O and HDO in different phases
531 (liquid: red line, solid: blue line) at different temperatures. The grey line is the ratio of
532 ^{18}O based on *Horita and Wesolowski* [1994].

533

534

Atmos. Chem. Phys. Discuss., https://doi.org/10.5194/acp-2018-596
Manuscript under review for journal Atmos. Chem. Phys.
Discussion started: 19 July 2018

Atmospheric Chemistry and Physics Discussions

535

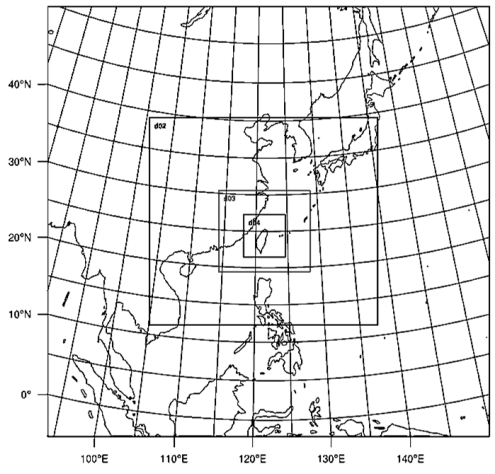

536

537 Figure 3. Map of the model domains for the simulations in this study. The resolutions

538 are 81, 27, 9 and 3 km in the outmost, 2nd, 3rd, and inmost domains, respectively.

539

Atmos. Chem. Phys. Discuss., https://doi.org/10.5194/acp-2018-596
Manuscript under review for journal Atmos. Chem. Phys.
Discussion started: 19 July 2018

Atmospheric Chemistry and Physics Discussions

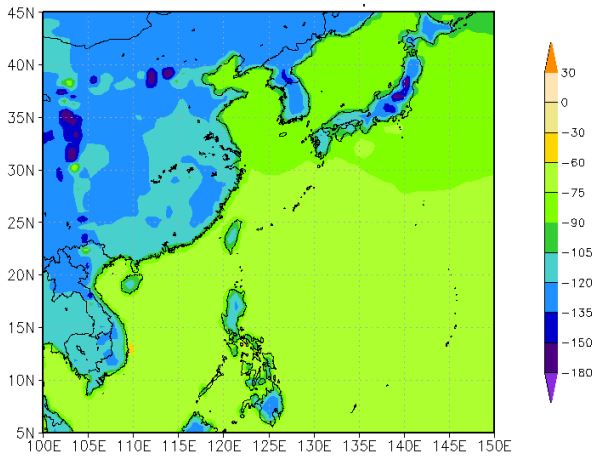

(a)

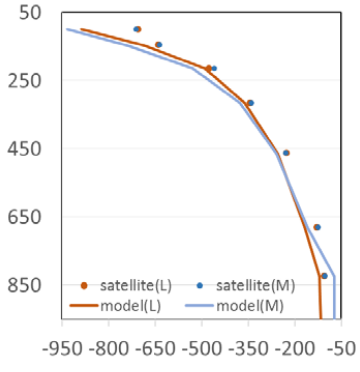

(b)

Figure 4. The initial distribution of water vapor δD (in ‰). (a) Surface distribution in the coarse domain; (b) vertical profiles fitted from satellite data (L for land and M for marine).

Atmos. Chem. Phys. Discuss., https://doi.org/10.5194/acp-2018-596
Manuscript under review for journal Atmos. Chem. Phys.
Discussion started: 19 July 2018

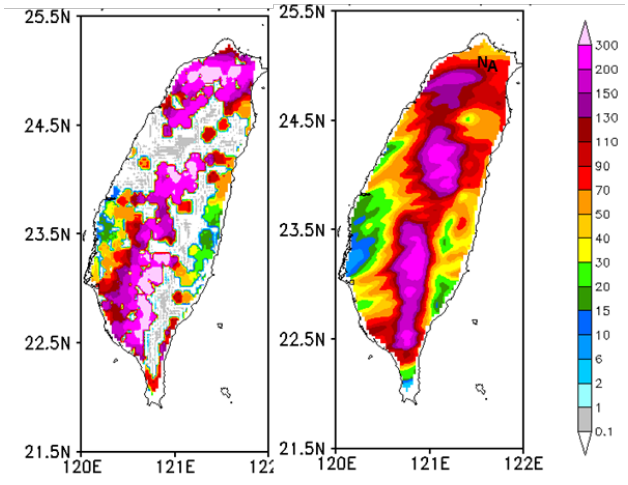

(a)

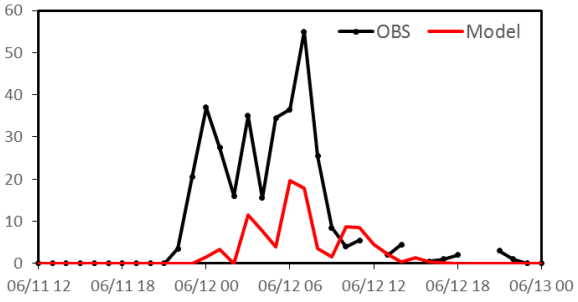

(b)

Figure 5. (a) Comparison between observed (left) and simulated (right) accumulated precipitation (mm/hr) in Taiwan on 12 June 2012. Mark N and A denotes the location of NTU and AS. (b) Simulated (red line) and observed (black line) precipitation at Taipei station on 11-13 June 2012.

Atmos. Chem. Phys. Discuss., https://doi.org/10.5194/acp-2018-596
Manuscript under review for journal Atmos. Chem. Phys.
Discussion started: 19 July 2018

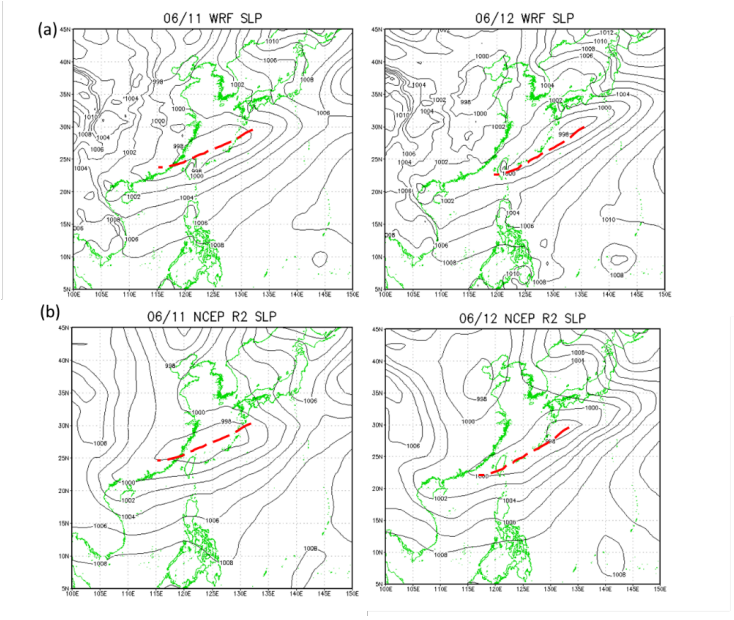

Figure 6. Comparison of (a) simulated sea level pressure (hPa) with (b) the NCEP reanalysis data on 11 June (left) and 12 June (right), 2012. Frontal position is indicated by the red-dashed lines.

Atmos. Chem. Phys. Discuss., https://doi.org/10.5194/acp-2018-596
Manuscript under review for journal Atmos. Chem. Phys.
Discussion started: 19 July 2018

Atmospheric Chemistry and Physics Discussions

561

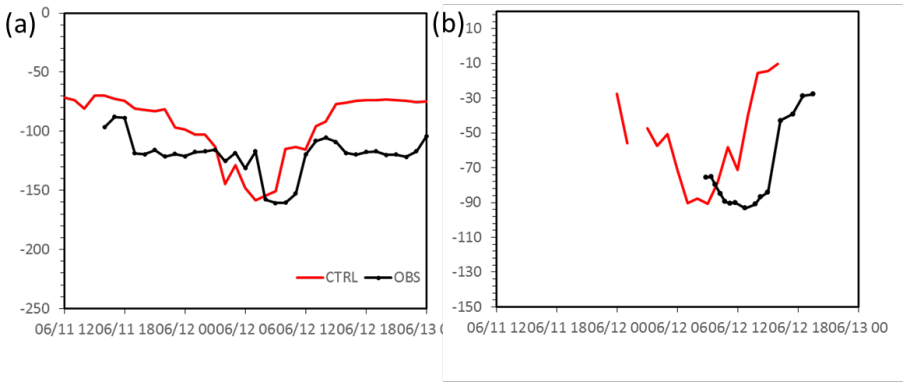

562

563 Figure 7. Simulated (CTRL: red line) and observed (black line) δD (in ‰) of (a) water
564 vapor at AS and (b) precipitation at NTU on 11-13 June 2012.

565

Atmos. Chem. Phys. Discuss., https://doi.org/10.5194/acp-2018-596
Manuscript under review for journal Atmos. Chem. Phys.
Discussion started: 19 July 2018

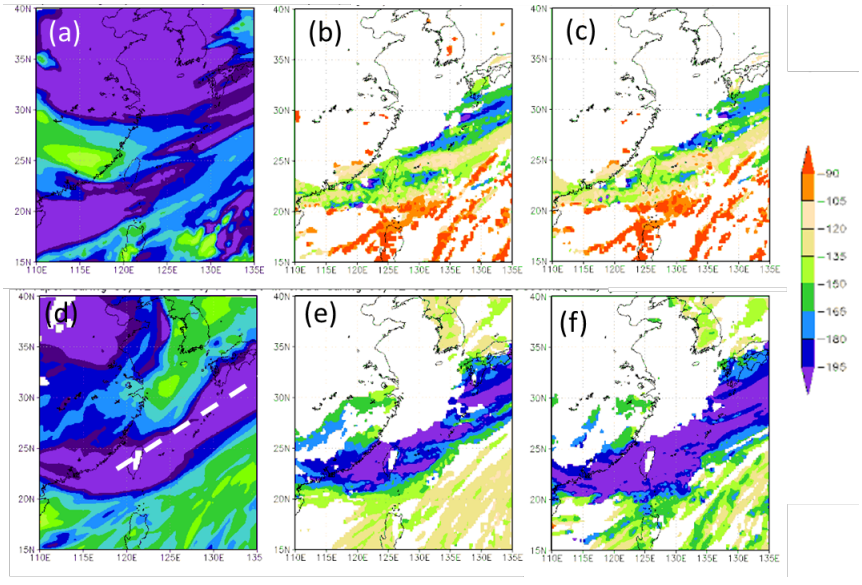

Figure 8. Simulated δD (in ‰) of water vapor (left), liquid-phase condensates including cloud- and rainwater (middle), and ice-phase condensates, including cloud ice, snow, and graupel (right) in the CTRL run at 500 hPa (a-c) and 850 hPa (d-f) on 12 June 2012.

Atmos. Chem. Phys. Discuss., https://doi.org/10.5194/acp-2018-596
Manuscript under review for journal Atmos. Chem. Phys.
Discussion started: 19 July 2018

Atmospheric Chemistry and Physics Discussions

572

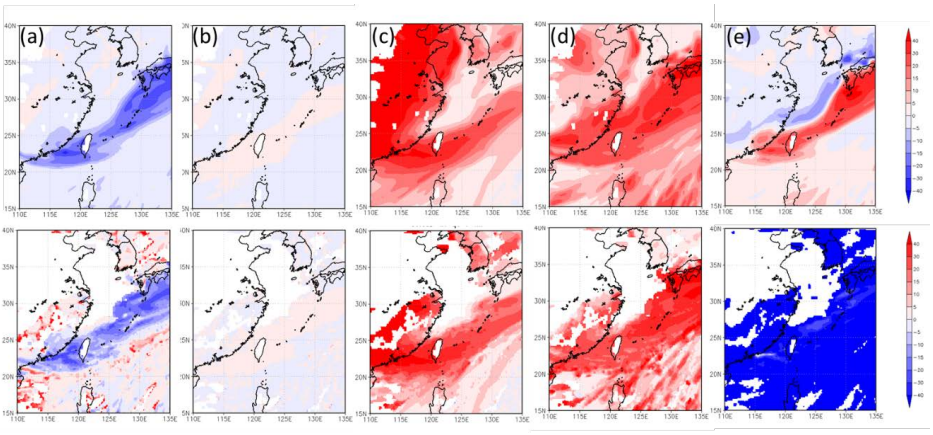

573

574 Figure 9. Difference in simulated δD (in ‰) of water vapor (upper) and liquid-phase
575 condensates, including cloud- and rainwater (lower), between CTRL and other runs:
576 (a) EQ-CTRL, (b) NoIce-CTRL, (c) NoLnd-CTRL, and (d) NoVh-CTRL, and (e) NoFrac-
577 CTRL, at 850 hPa on 12 June 2012.

578

579

Atmos. Chem. Phys. Discuss., https://doi.org/10.5194/acp-2018-596
Manuscript under review for journal Atmos. Chem. Phys.
Discussion started: 19 July 2018

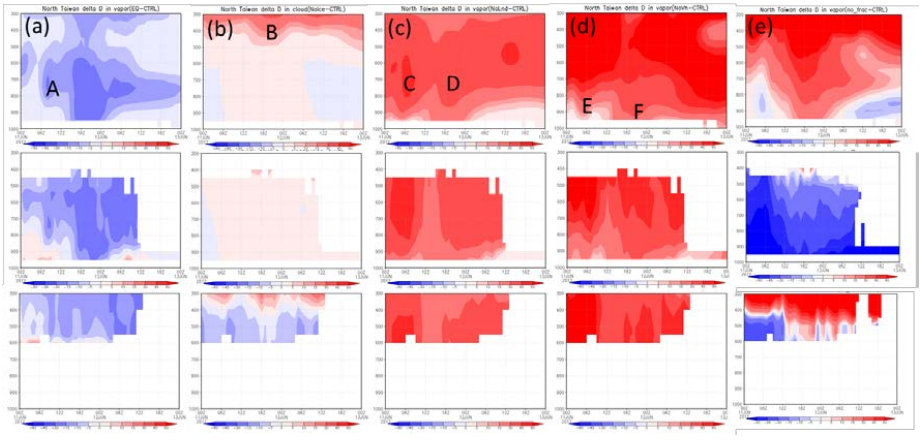

Figure 10. Vertical distribution of simulated water vapor δD in ‰ (top), liquid-phase water (cloud- and rainwater, middle), and ice-phase water (snow and graupel, bottom) over northern Taiwan in different simulations: (a) EQ-CTRL, (b) NoIce-CTRL, (c) NoLnd-CTRL, (d) NoVh-CTRL,and (e) NoFrac-CTRL on 11-12 June 2012.

Atmos. Chem. Phys. Discuss., https://doi.org/10.5194/acp-2018-596
Manuscript under review for journal Atmos. Chem. Phys.
Discussion started: 19 July 2018

Atmospheric Chemistry and Physics Discussions

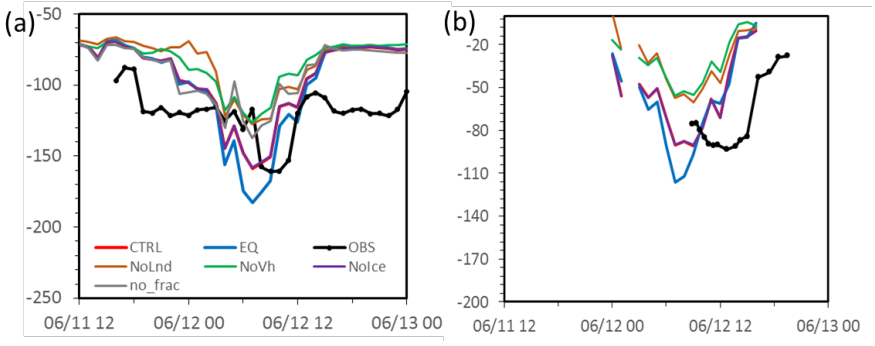

Figure 11. Time evolution of (a) water vapor δD (in ‰) and (b) precipitation δD (in ‰)at Nankang, Taipei, during June 11-13, 2012. Measured values are shown in black lines, whereas the simulations include the control run (CTRL, red line), thermodynamic equilibrium run (EQ, blue line), no-ice run (NoIce, purple line), no-land run (NoLnd, orange line), constant initial vertical profile run (NoVh, green line), and no fractionation run (no_frac, grey line).

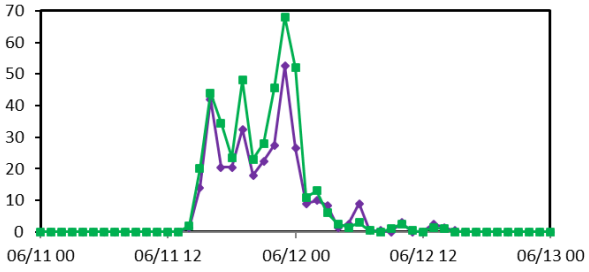

596

597 Figure 12. Precipitation at NanGang (purple line) and GongGuan (green line) Stations
598 on 11-13 June 2012.

599

600